

Facile synthesis of 3-D composites of MnO₂ nanorods and holey graphene oxide for supercapacitors

Lixin Wang¹ · Da Deng¹ · Steven O. Salley¹ · K. Y. Simon Ng¹

Received: 5 December 2014 / Accepted: 9 June 2015 / Published online: 25 June 2015
© Springer Science+Business Media New York 2015

Abstract A facile method was developed to prepare MnO₂/holey graphene oxide (MnO₂/HGO) materials based on graphene oxide (GO) flakes for supercapacitor applications. FESEM images show that MnO₂ nanorods were formed on the surface of HGO flakes, serving as spacers and preventing the HGO layers from stacking. This provides pathways between the layers for the electrolyte to access the bulk active materials. By introducing the high intrinsic capacitance MnO₂ nanorods together with the modified 3-D structure, capacitance increases to 71.0 F/g compared with 30.0 F/g of GO. More pathways were created by nitric acid etching holes on the surface of the GO. This 3-D holey MnO₂/HGO structure achieves a capacitance of 117.45 F/g, which is 1.65 times higher than that of MnO₂/GO composite and 3.9 times higher than that of GO only. BET surface area, XRD, and AC impedance were also used to analyze the possible reasons for the enhanced electrochemical performance.

Introduction

The supercapacitor, an energy storage device that bridges the gap of energy and power density between secondary batteries and conventional capacitors, has spurred new and interesting research by many groups. One of the key issues is the improvement in the energy density ($E = \frac{1}{2} CV^2$). A direct way to improve energy density is to improve the

capacitance. While the capacitance is proportional to the electrode surface area, numerous carbon-based materials are reported to fulfill this requirement, such as graphene, activated carbon, carbon aerosols, and carbon nanotubes [1–3]. On top of these different kinds of carbon materials, a variety of structures are designed to increase the integrity and conductivity while increasing the electrolyte accessible surface. Examples of these are 1-D carbon nanotubes, rods and wires [4], 2-D graphene sheets [5] and graphene papers [6], and 3-D carbon forests [7] of either a pure material or composites. For example, Kim et al. [8] reported a 3-D architecture of graphene and carbon nanotubes with a capacitance of 490.3 $\mu\text{F}/\text{cm}^2$, compared to 100 $\mu\text{F}/\text{cm}^2$ [9] for graphene-only electrodes at a fast charge–discharge rate. They concluded that the carbon nanotubes, grown by chemical vapor deposition between graphene layers, alleviated the graphene self-aggregation and therefore enhanced the current pathway between the graphene layers. Jiang et al. [9] summarized the studies on graphene and carbon nanotube-based 3-D porous architectures. They concluded that the 3-D configuration provides hierarchical porous channels that enhance the ion diffusion and accessibility of electrolyte to the electrode surface. The importance of tailoring pore sizes in the mesopore regime to optimize the electrochemical performance was also pointed out in their study.

In addition to electrical double layer capacitance that is mainly determined by surface area, pseudocapacitance that is based on faradic mechanisms (electrosorption, redox reactions, and intercalation) is also a booster of the capacitance [10]. Among these pseudocapacitive materials, transition metal oxides are considered to be the most promising choices, due to their superiority in high intrinsic capacitance, compared to their conductive polymer counterparts. RuO₂ [11], MnO₂ [12, 13], CoO₂, and V₂O₅ [14]

✉ K. Y. Simon Ng
sng@wayne.edu

¹ Department of Chemical Engineering and Materials Science, Wayne State University, 5050 Anthony Wayne Drive, Detroit, MI 48202, USA

are all reported to be able to provide high pseudocapacitance. However, due to the nonconductive nature of the metal oxides, electrodes of this kind are usually made into a very thin film of less than several hundred nanometers so that electrons can still transfer effectively through the electrode [15, 16]. As a result, it is usually not straightforward to achieve a high enough volumetric energy density for commercial applications. To alleviate the conductivity issue, the metal oxides are integrated with highly conductive carbon materials at a certain ratio. For example, He et al. [17] electrochemically deposited MnO_2 on 3-D graphene networks to enhance the capacitance of 130 F/g of the composite while still maintaining a preferable conductivity. They believe that the 3-D graphene network serves as a highway for electron transfer and provides easy access for electrolyte ions. Supercapacitors made from bulk materials often have much lower capacitances compared to the ones with thin film electrodes. Liu et al. achieved a capacity of 193.8 F/g with bulk graphene/manganese oxides composites [18]; electrodes made from graphene paper and metal oxide composites reported by Huang et al. exhibited a capacity of 127.5 F/g [19]. These approaches usually need to trade off between the intrinsic capacitance and conductivity of the composites, and require complex and energy-consuming preparation processes. In a word, although many delicate structures have been reported to show very promising capacitance, they are either not able to form a thickness to achieve an acceptable energy density, or are not economically viable for mass production.

In our previous work [20], MnO_2 nanorods were successfully grown from the surface of graphene. The effects of reaction time and temperature on the morphology of the MnO_2 nanorods were investigated. The morphology was, in turn, correlated to the electrochemical performance of the MnO_2 and commercial graphene composites. The optimized reaction conditions of 24-h reaction time and 100 °C reaction temperature were identified and used in this study.

In this paper, a novel 3-D MnO_2/HGO composite is prepared in a simple acid-treating process [21] followed

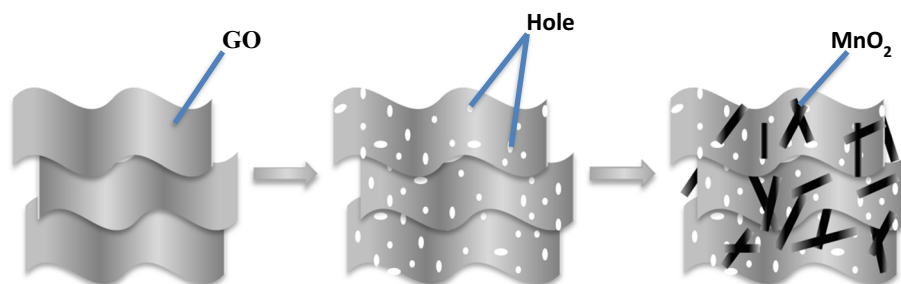
by a hydrothermal reaction. The formation process is illustrated in Fig. 1. Holes are first made on the surface of GO sheets by acid etching to form holey graphene oxide (HGO), and then MnO_2 nanorods are grown from the surface of the HGO. This 3-D network synergistically enhances the pathways for the electrolyte to access the surface of the bulk active material. The holes on the HGO nanosheets provide even more cross-plate pathways for the electrolyte in the direction vertical to the surface [21]. The HGO nanosheets provide highly active surface area and high conductivity, while also serving as nanoscale current collectors, a substrate to support MnO_2 nanorods, and a conductivity enhancer to augment the overall micro-scale electrical integration of the electrode. MnO_2 nanorods have the dual role of providing high intrinsic capacitance and serving as spacers in the 3-D structure to prevent soft and thin HGO sheets from stacking back together and losing their active surface areas. The elevated pathways provided by the 3-D holey structure, together with the introduction of high intrinsic MnO_2 nanorods, resulted in an elevated capacitance for the 3-D MnO_2/HGO composite.

Method and approach

HGO preparation

GO was prepared as reported in Ref. [22]. HGO was prepared similarly as reported in [21], while a higher acid ratio and longer etching time were used to enhance the etching effects. The GO suspension was mixed with HNO_3 (Sigma-Aldrich, 70 wt%) at a GO to HNO_3 ratio of 3:1. The mixture was placed in an ultrasonic bath (Branson 2510, maximum power: 100 W) at four different time periods of 0.5, 1, 2, and 3 h to etch the GO flakes. A rinsing process using DI water was followed, until the pH value of the mixture reached 7, to remove the excess acid. The suspension was then condensed by centrifugation, and the supernatant liquid was decanted. The weight ratio of the HGO in the suspension is 1.90 %.

Fig. 1 Illustration of the formation of 3-D MnO_2/HGO



MnO₂/HGO composite preparation

MnO₂/HGO composite was synthesized as reported in our previous work [20]. In a typical procedure, a suspension that contains 50 mg HGO was mixed with 25 mL aqueous solution of KMnO₄ (0.1 M), K₂SO₄ (0.1 M), and K₂S₂O₈ (0.1 M). The mixture was diluted to 75 mL, placed into a Teflon-lined autoclave, and kept at 100 °C for 24 h. The supernatant liquid was then decanted, and the solid product at the bottom of the autoclave was collected. The sediment was washed with DI water five times to completely remove the residual salts. The product was then dried in a vacuum oven at 100 °C for 12 h.

Electrochemical testing setups

The as-prepared composite powders were dispersed in *N*-methyl-2-pyrrolidone (NMP) solution with a polyvinylidene difluoride (PVDF) binder (composites to PVDF mass ratio of 9:1). Then, pre-cleaned Ni foam (30–40 mg, 0.25 × 0.25 cm², 0.165 cm in thickness) was immersed into the slurry to load the active materials. The coated Ni foam was taken out of the slurry, kept at 80 °C for 4 h, and then dried at 110 °C for 12 h in a vacuum oven. The dry electrode was then pressed through a rolling mill to enhance the contact between the active material and the substrate. The final thickness of the electrode was 0.089 cm. The average loading amount of MnO₂/HGO composite on the Ni foam was about 2 mg.

The electrochemical performance was tested using a standard three-electrode setup, with MnO₂/HGO composite as the electrode material, a Pt wire serving as the counter electrode, and an Ag/AgCl electrode as the reference electrode. MnO₂/HGO composite-coated Ni foam was hung from a Ni wire as the working electrode in 1 M Na₂SO₄ aqueous solution as the electrolyte.

Characterization

The crystal structures of the samples were examined using a Rigaku RU 200B X-ray diffractometer, and a field-emission scanning electron microscope (FESEM, JSM-7600F at 15 kV) was used to study the morphology of the composites. Cyclic voltammetry testing was conducted using a Gamry 3000 Potentiostat (Gamry Instruments, Warminster, PA). The scan rate used in cyclic voltammetry was 0.5 mV/s with a scan voltage window between 0 and 0.8 V. The AC impedance measurement was conducted using a Parstat 2273 electrochemical system (Princeton Applied Research) with frequency range of 0.5 mHz to 10 kHz. Raman spectra were obtained using Triax 550 (Horiba Jobin Yvon, Edison, NJ). Brunauer–Emmett–Teller (BET) surface area measurements were carried out

using a Tristar 3020 surface area analyzer with N₂ as the analysis gas. The thermogravimetric analysis (TGA) was tested using a Model TA Instruments 2960 (New Castle, DE) at a heating rate of 10 °C/min in air.

Results and discussion

XRD and Raman characterization

The powder X-ray diffraction patterns of the as-prepared samples are depicted in Fig. 2. The XRD pattern of the GO sample shows a typical graphene oxide peak at 13° as shown in Fig. 2a. The XRD patterns of the MnO₂/GO composite (Fig. 2b) and MnO₂/HGO composite (Fig. 2c) show very similar major α -MnO₂ peaks at $2\theta = 12.45^\circ$, 17.65°, 28.25°, 37.35°, 41.55°, 49.35°, and 59.55°. All of the diffraction peaks are indexed to the tetragonal phase (space group I4/m) with the lattice constants of $a = 9.8172 \text{ \AA}$ and $c = 2.8582 \text{ \AA}$ (JCPDS 44-0141) [23]. The sharp and well-defined peaks indicate the crystallinity of the as-prepared MnO₂/GO and MnO₂/HGO composites. There is no significant difference in the XRD spectra between the two samples. The TGA results show 75.9 and 74.8 wt% of MnO₂ in MnO₂/GO and MnO₂/HGO samples, respectively. The TGA curve of MnO₂/GO is shown in Fig. 3 as an example. The similarity in crystal structure and MnO₂ percentages suggest that the differences in the electrochemical performances are more likely to be from the morphological differences.

Figure 4a and b show the Raman spectra of GO and HGO. Both of the samples exhibit D, G, and broad 2D peaks at around 1348, 1590, and 2600 cm⁻¹, indicating the presence of graphene oxide. The broad and less intense 2D band indicates that the graphene oxide samples have a very thin layer. The intensity ratio of the D band and G band (D/

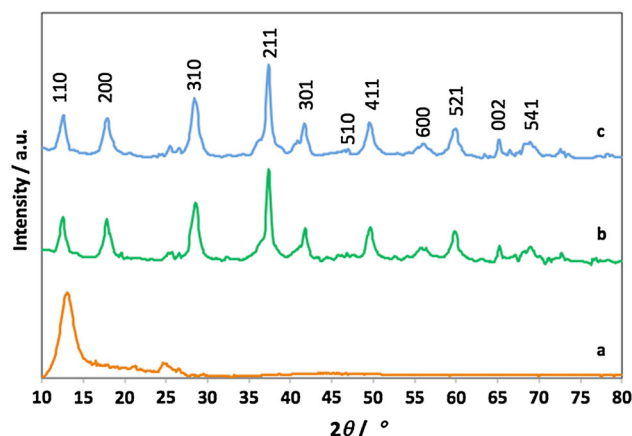


Fig. 2 XRD patterns of the **a** GO, **b** MnO₂/GO, and **c** MnO₂/HGO

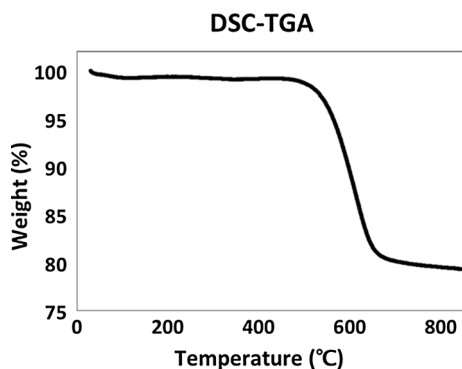


Fig. 3 TGA curve of MnO₂/GO

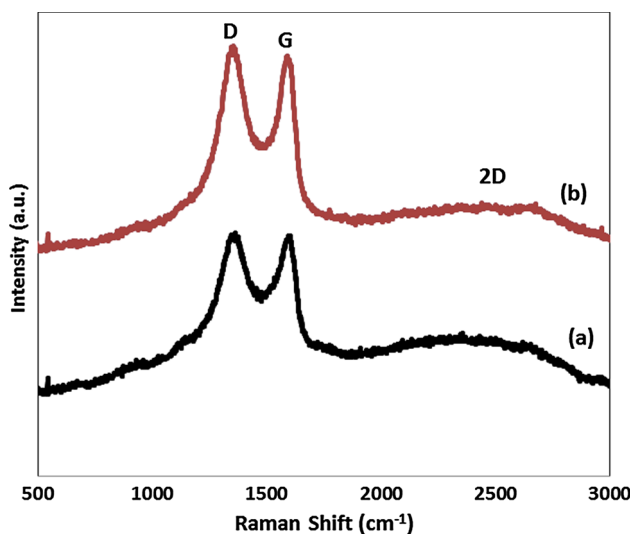


Fig. 4 Raman spectra of a GO b HGO

G) for HGO is 1.09, compared to that of 1.03 for GO, suggesting the successful introduction of defects by the acid treatment.

Morphology study

The morphology of the four samples etched at 0.5, 1, 2, and 3 h were studied using field-emission scanning electron microscopy. As shown in Fig. 5, holes with diameters of around 100 nm were clearly observed in all four samples at different etching time periods. Interestingly, there are no significant differences among the four samples, prepared at the four different etching time periods, regarding the number of holes and the size of the holes. The hole sizes are in agreement with that reported by Zhao [21] under similar conditions. In comparison, MnO₂ nanorods prepared under the same hydrothermal conditions, but without graphene, show a very different morphology (Fig. 5e). These nanorods are irregular rods that are much larger than the ones prepared with HGO. Holes of similar size and

distribution are also found on the holey graphene sample without MnO₂ nanorods, as shown in Fig. 5f.

It is shown in Fig. 6a that GO has a flat and non-porous surface consisting of GO flakes stacked together. MnO₂/GO composite, on the other hand, shows a looser 3-D structure compared to that of pure GO, where nanorods grow from the GO surface (Fig. 6b). With MnO₂ nanorods as spacers between the GO flakes, the 3-D structure provides an easier pathway for the electrolyte to access the surface of the active materials. In order to further increase the surface area exposed to electrolyte and enhance the electrolyte penetration through the integrated electrodes, holes were made by acid etching on the surface of the GO before growing MnO₂. The resulting 3-D structure of the MnO₂/HGO composite is shown in Fig. 6c, at two different magnifications. Holes with diameters of around several hundred nanometers are clearly observed (indicated by the arrows), scattered evenly on the surface of the HGO. The MnO₂ nanorods were highlighted by dotted lines in Fig. 6c. In addition to the pathways made by the MnO₂ nanorod spacers between the HGO flakes, the holes provide further possible pathways through the HGO flakes for the electrolyte to have access to the bulk of the active materials [21]. Therefore, more MnO₂ nanorod spacers in the bulk can also contribute to the reversible charge storage with enhanced electrochemical performance, as compared to the tightly packed GO electrodes. Furthermore, the holes also make it possible for the MnO₂ nanorods to pass through the HGO flakes, rather than staying in between the flakes. In other words, the MnO₂ nanorods are not necessarily parallel to the local HGO sheets, but instead are in a 3-D orientation against the surface of the local HGO sheets, which will provide more steric scaffold for the 3-D structured composite.

Electrochemical performances

Figure 7 shows the CV curves of the as-prepared samples. The capacitances calculated from the CV curves are summarized in Fig. 8. Among the MnO₂/HGO samples with different etching times, the sample with a 3-h etching time shows the highest capacitance of 117 F/g. Despite the negligible differences in hole sizes and distributions observed from FESEM images, the capacitances show a slightly increasing trend with the increased acid etching time from 85.7 F/g at 0.5 h to 117 F/g at 3 h.

On the other hand, capacitance differences between GO, MnO₂/GO, and MnO₂/HGO can be attributed to the differences in the surface areas and impedances of the materials. Table 1 summarizes the results, along with the specific surface areas for the materials. The GO sample, with a surface area of 408 m²/g, shows a limited capacitance of 30 F/g, due to agglomeration and restacking of GO

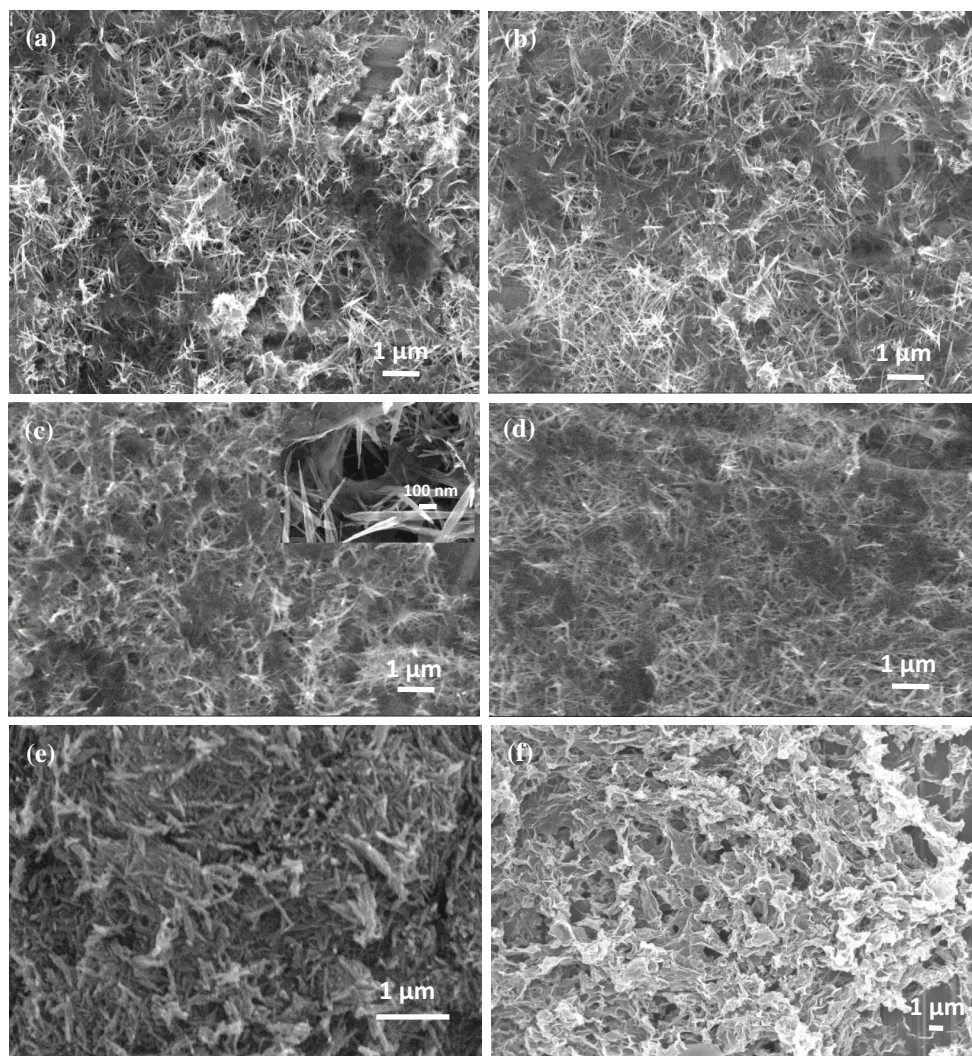


Fig. 5 FESEM images of MnO₂/HGO composites at different etching times: **a** 0.5 h, **b** 1 h, **c** 2 h, and **d** 3 h, **e** MnO₂ and **f** HGO

layers, which is similar to the findings by Wang et al. [5]. The HGO sample suffered from severe aggregation during the drying process, which resulted in a low surface area of 6.3 m²/g, in contrast to less aggregation of GO during the drying process. The severe aggregation may be attributed to the loss of functional groups (such as OH⁻, which help keep the GO sheets apart) on the GO surface during acid etching. To avoid this aggregation problem, MnO₂ nanorods were grown in the HGO suspension in order to space the HGO sheets from stacking back together. The integration of MnO₂ nanorods within the layers of GO increases the intrinsic capacitance of the composite while preventing GO restacking and gives more accessibility to the bulk. A higher capacitance of 71 F/g was obtained, even though the surface area of the MnO₂/GO is much smaller (75.20 m²/g) than that of GO (408 m²/g). A similar capacitance value of 90 F/g has also been reported using bulk MnO₂/GO as the active materials [17]. With further

engineering of the 3-D structure by etching holes on the surface of GO, the capacitance increased to 117 F/g even though the specific surface area only increased slightly to 86.06 m²/g. There is a significant increase of almost 60 % compared to MnO₂/GO composite. This result is in agreement with Vaquero's report that mesopores of the materials facilitate ion accessibility and adsorption on the surface [24].

The EIS curves of GO, MnO₂/GO, and MnO₂/HGO composites are depicted in Fig. 9. The intercept of the Nyquist plot with the real part (Z_{rel}) corresponds to the equivalent series resistance (ESR) of the system, which includes the intrinsic ohmic resistance of the electrode material and the ionic resistance of the electrolyte [17, 25]. The ESR value of MnO₂/GO increases to 2.1 Ω, compared to 1.1 Ω for GO. The increase in ESR can be attributed to the integration of low-conductivity MnO₂ nanorods into GO layers. On the other hand, the etching holes on the surface of

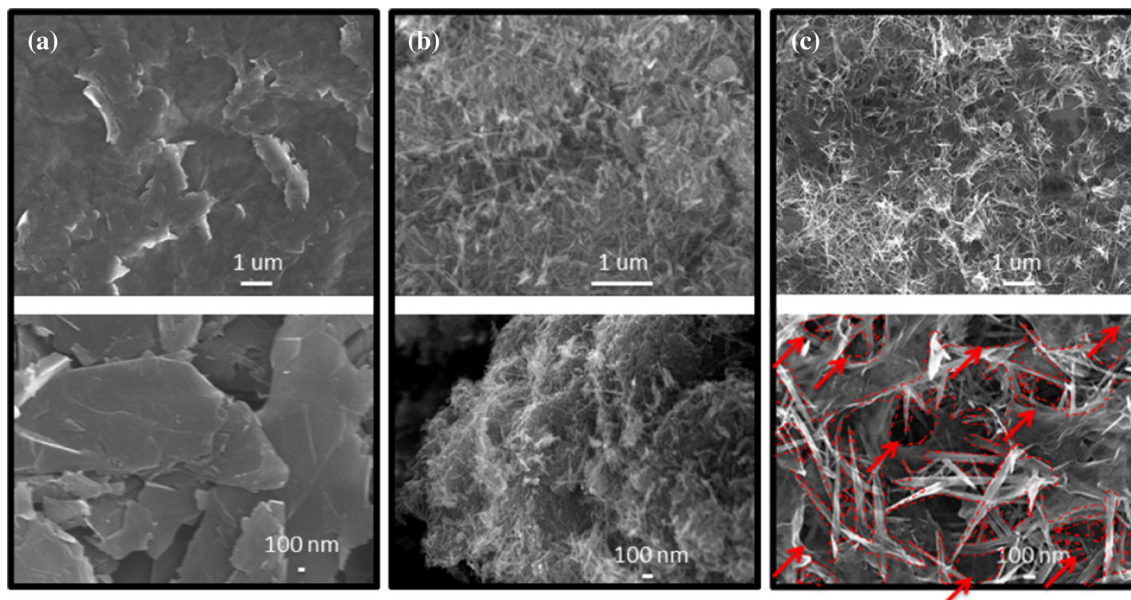


Fig. 6 FESEM images of **a** GO, **b** MnO₂/GO composite, **c** MnO₂/HGO composite at different magnifications

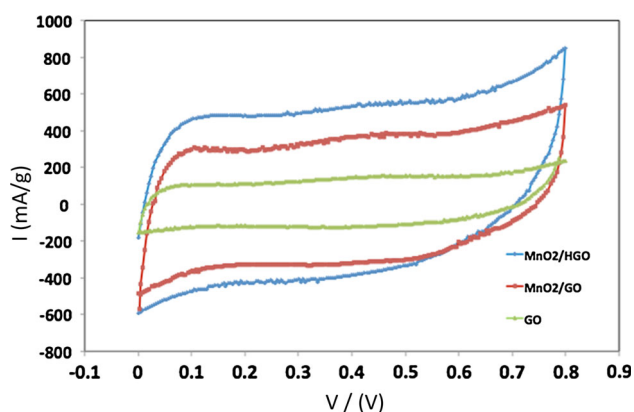
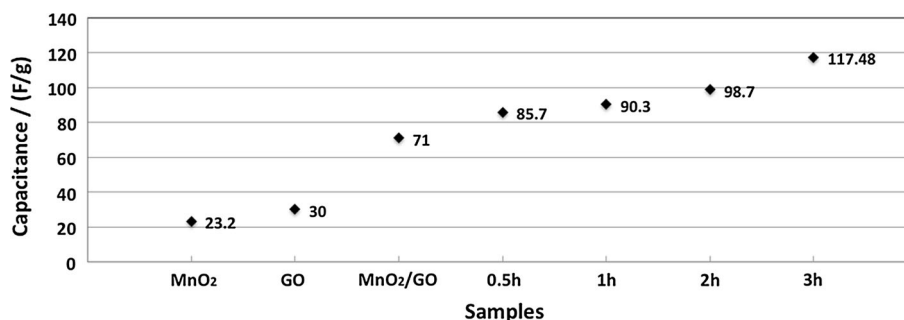


Fig. 7 CV curves of GO, MnO₂/GO composite, and MnO₂/HGO composite at 5 mV/s scan rate

the HGO break the carbonaceous framework and cause partial detachment and removal of carbon atoms from the GO sheet [21]. Thus, the impedance of the MnO₂/HGO increases to 3.5 Ω, compared to 2.1 Ω for the MnO₂/GO

Fig. 8 Capacitance changes of MnO₂, GO, MnO₂/GO composite, MnO₂/HGO with etching time of 0.5, 1, 2, and 3 h

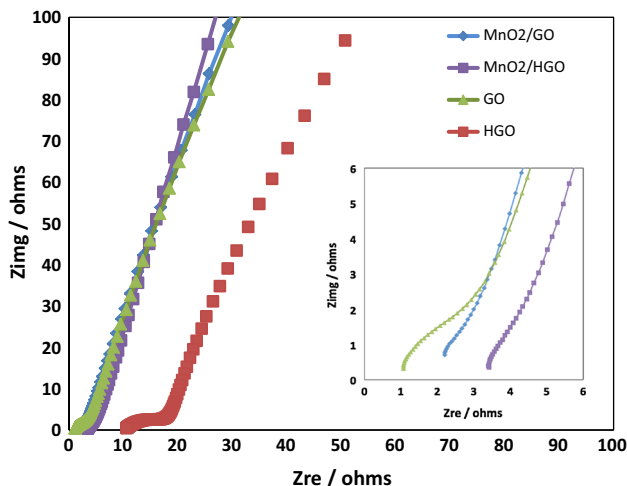


composite. Interestingly, the impedance of HGO (14.1 Ω) is more than four times higher than that of MnO₂/HGO. This unexpected high impedance might be due to higher resistance at the grain boundaries, resulting from severe aggregation during the drying process. Even with PVDF binder, the aggregated particles of HGO are hard to attach to the current collector. The difficulty of attaching might be another factor that contributes to the high impedance.

The diameter of the semicircle at the high-frequency region can be used to estimate the charge transfer resistance (R_{ct}) [26]. As shown in Fig. 9, the much smaller semicircle of MnO₂/GO and MnO₂/HGO indicate a smaller R_{ct} compared to that of GO. The smaller R_{ct} is associated with the increased contact area at the electrode–electrolyte interface due to the 3-D network [27]. The more inconspicuous loop of MnO₂/HGO in the high- to mid-frequency region, which leads to a more vertical low-frequency curve, indicates a well-connected interface of electrolyte ions and the electrode [25]. The enhanced electrolyte ion diffusion and connection leads to high capacitance of 117 F/g compared

Table 1 Electrochemical properties and specific surface area of the tested materials

| Material | Capacitance (F/g) | Impedance (Ω) | Specific surface area (m^2/g) |
|---------------------------|-------------------|------------------------|---|
| GO | 30.0 | 1.1 | 408 |
| HGO | 12.5 | 14.1 | 6.3 |
| MnO_2/GO | 71.0 | 2.5 | 75.20 |
| MnO_2/HGO | 117.48 | 3.5 | 86.06 |

**Fig. 9** EIS Curves of GO, MnO_2/GO composites and MnO_2/HGO composites

to 71 F/g for MnO_2/GO . The elevated capacitance of MnO_2/GO , compared to that of GO, is likely due to lower R_{ct} , since there is no significant difference in the ion diffusion between MnO_2/GO and GO based on the EIS curves.

Conclusion

A convenient, economical, and easy-to-scale-up method of preparing 3-D materials for supercapacitors is reported. The MnO_2 nanorods act as spacers in between the HGO layers, minimizing agglomeration and stacking of layers. Although the specific surface area decreases from 408 to 76.1 m^2/g , the capacitance of the MnO_2/GO composite increased by 57.7 % due to the introduction of MnO_2 and the 3-D network. Furthermore, etching holes on the surface of GO flakes further optimize the 3-D structure and create more pathways for the electrolyte to penetrate into the bulk materials. Therefore, a further increase of 64.8 % was achieved, even though the impedance of the composite was higher than that of the MnO_2/GO composite due to the disruption of the conductive GO surface.

Acknowledgement Financial support from the Department of Energy (Grant DEFG36-05GO85005) for this research is gratefully acknowledged.

References

1. Markoulidisa F, Leia C, Lekakoua C, Duffb D, Khalilb S, Mar-toranac B, Cannavaroc I (2014) A method to increase the energy density of supercapacitor cells by the addition of multiwall carbon nanotubes into activated carbon electrodes. *Carbon* 68:58–66
2. Mateyshina Y, Ulihin A, Samarov A, Barnakov C, Uvarov N (2013) Nanoporous carbon-based electrode materials for super-capacitors. *Solid State Ion* 251:59–61
3. Mezavilla S, Zanella C, Aravind PuR, Yolpe CD, Soraru GD (2012) Carbon xerogels as electrodes for supercapacitors. The influence of the catalyst concentration on the microstructure and on the electrochemical properties. *J Mater Sci* 47:7175–7180. doi:10.1007/s10853-012-6662-1
4. Tao J, Liu N, Ma W, Ding L, Li L, Su J, Gao Y (2013) Solid-state high performance flexible supercapacitors based on polypyrrolone- MnO_2 -carbon fiber hybrid structure. *Sci Rep* 3:2286. doi:10.1038/srep02286
5. Wang Y, Shi Z, Huang Y, Ma Y, Wang C, Chen M, Chen Y (2009) Supercapacitor devices based on graphene materials. *J Phys Chem C* 113:13103–13107
6. Yao W, Wang J, Li H, Lu Y (2014) Flexible α - MnO_2 paper formed by millimeter-long nanowires for supercapacitor electrodes. *J Power Sources* 247:824–830. doi:10.1016/j.jpowsour.2013.09.039
7. Hu J, Kang Z, Li F, Huang X (2014) Graphene with three-dimensional architecture for high performance supercapacitor. *Carbon* 67:221–229. doi:10.1016/j.carbon.2013.09.085
8. Kim Y-S, Kumar K, Fisher FT, Yang E-H (2012) Out-of-plane growth of CNTs on graphene for supercapacitor applications. *Nanotechnology* 23:015301–015308. doi:10.1088/0957-4484/23/1/015301
9. Jiang H, Lee PS, Li C (2013) 3D carbon based nanostructures for advanced supercapacitors. *Energy Environ Sci* 6:41–53. doi:10.1039/c2ee23284g
10. Conte M (2010) Supercapacitors technical requirements for new applications. *Fuel Cells* 10(5):806–818
11. Sopic S, Rokovic MK, Mandic Z, Róka A, Inzelt G (2011) Mass changes accompanying the pseudocapacitance of hydrous RuO_2 under different experimental conditions. *Electrochim Acta* 56:3543–3548. doi:10.1016/j.electacta.2010.10.035
12. Li Z-S, Wang H-Q, Huang Y-G, Li Q-Y, Wang X-Y (2010) Manganese dioxide-coated activated mesocarbon microbeads for supercapacitors in organic electrolyte. *Colloids Surf A* 366:104–109. doi:10.1016/j.colsurfa.2010.05.031
13. Su L, Gong L, Lü H, Xü Q (2014) Enhanced low-temperature capacitance of MnO_2 nanorods in a redox-active electrolyte. *J Power Sources* 248:212. doi:10.1016/j.jpowsour.2013.09.047
14. Yang J, Lan T, Liu J, Song Y, Wei M (2013) Supercapacitor electrode of hollow spherical V_2O_5 with a high pseudocapacitance in aqueous solution. *Electrochim Acta* 105:489–495. doi:10.1016/j.electacta.2013.05.023
15. Nakayama M, Tanaka A, Sato Y, Tonosaki T, Ogura K (2005) Electrodeposition of manganese and molybdenum mixed oxide thin films and their charge storage properties. *Langmuir* 21:5907–5913

16. Dubal DP, Dhawale DS, Salunkhe RR, Lokhande CD (2010) A novel chemical synthesis of Mn_3O_4 thin film and its stepwise conversion into birnessite MnO_2 during super capacitive studies. *J Electroanal Chem* 647:60–65
17. He Y, Chen W, Li X, Zhang Z, Fu J, Zhao C, Xie E (2013) Freestanding three-dimensional graphene/ MnO_2 composite networks as ultralight and flexible supercapacitor electrodes. *ACS Nano* 7:174–182. doi:[10.1021/nm304833s](https://doi.org/10.1021/nm304833s)
18. Liu Y, He D, Wu H, Duan J, Zhang Y (2015) Hydrothermal self-assembly of manganese dioxide/manganese carbonate/reduced graphene oxide aerogel for asymmetric supercapacitors. *Electrochim Acta* 164:154–162
19. Huang Y, Zhu M, Meng W, Fu Y, Wang Z, Huang Y, Pei Z, Zhi C (2015) Robust reduced graphene-oxide paper fabricated by household non-stick frying pan: large-area freestanding flexible substrate for supercapacitor. *RSC Adv* 5:33981–33989. doi:[10.1039/c5ra02868j](https://doi.org/10.1039/c5ra02868j)
20. Wang L, Deng D, Ng KYS (2013) Facile one-step synthesis of MnO_2 nanowires on graphene under mild conditions for application in supercapacitors. *J Mater Sci* 48(18):6410–6417. doi:[10.1007/s10853-013-7441-3](https://doi.org/10.1007/s10853-013-7441-3)
21. Zhao X, Hayner CM, Kung MC, Kung HH (2011) Flexible holey graphene paper electrodes with enhanced rate capability for energy storage applications. *ACS Nano* 5(11):8739–8749
22. Lee JK, Smith KB, Hayner CM, Kung HH (2010) Silicon nanoparticles–graphene paper composites for Li ion battery anodes. *Chem Commun* 46:2025–2027
23. Balakrishnan A, Subramanian KRV (2014) Nanostructured ceramic oxides for supercapacitor applications. CRC Press, New York
24. Gamby J, Taberna PL, Simon P, Fauvarque JF, Chesneau M (2001) Studies and characterisations of various activated carbons used for carbon/carbon supercapacitors. *J Power Sources* 101:109–116
25. Zhang L, Zhang F, Yang X, Long G, Wu Y, Zhang T, Leng K, Huang Y, Ma Y, Yu A, Chen Y (2013) Porous 3D graphene-based bulk materials with exceptional high surface area and excellent conductivity for supercapacitors. *Sci Rep* 3:1408–1416
26. Wang Y, Guo CX, Liu J, Chen T, Yang H, Li CM (2011) CeO_2 nanoparticles/graphene nanocomposite-based high performance supercapacitor. *Dalton Trans* 40:6388–6391
27. Choi BG, Yang M, Hong WH, Choi JW, Huh YS (2012) 3D macroporous graphene frameworks for supercapacitors with high energy and power densities. *ACS Nano* 6(5):4020–4028. doi:[10.1021/nm3003345](https://doi.org/10.1021/nm3003345)